Modeling of Chromium Oxide Separation to Liquid Slag and the Effect of Top Slag on Decarburization in an AOD Converter

Nils Andersson, Anders Tilliander, Lage T. I. Jonsson, Pär G. Jönsson*

Div. Applied Process Metallurgy, KTH Royal Institute of Technology, 100 44 Sweden

Abstract: The AOD (Argon-Oxygen Decarburization) converter is a common reactor for refining stainless steel grades. The process has high productivity and yields good reduction of carbon and sulfur with small chromium losses. Since stainless steel have high demands on alloying elements as well as keeping losses to a minimum, these parts need to be studied further. A high-temperature thermodynamics model has been coupled with a CFD (Computational Fluid Dynamics) model describing the fluid flow. The boundary conditions were chosen based on data for an industrial AOD converter and they have been reported in literature earlier. With this model, separation of chromium oxide to liquid slag and the effect of the top slag amount during decarburization have been investigated. The liquid slag was considered for the uptake of chromium oxide, while the top slag was only considered for its contribution to increase the metallostatic pressure. The results suggest that separation of chromium oxide to liquid slag inhibits the decarburization. The same conclusion can be drawn with respect to the amount of solid top slag. However, the effects are rather small so they do not affect the process noteworthy. Overall, it is concluded that the impact of the top slag and liquid slag on the reactions should be investigated further.

Key words: aod, modeling, cfd, slag, separation

1. Introduction

Stainless steel is produced by melting scrap in an electric arc furnace, then refining the molten scrap in a converter before casting. Inexpensive scrap contains high concentrations of carbon, which results in bad mechanical properties for stainless steel. Thus, it is important to reduce the carbon content in an efficient way to produce a high quality stainless steel. A process with high carbon removal efficiency and low chromium consumption is called an Argon Oxygen Decarburization process (AOD). The most common operation scheme of an AOD is divided into several stages: decarburization, reduction and desulfurization. The decarburization stage is further divided into different steps where the oxygen-argon ratio is decreased in each step. The AOD converter operates at high temperatures and with violent stirring, which makes it hard to carry out experiments to gain further knowledge about how the process works.

Earlier Ternstedt et al. [1] investigated the influences of AOD slag on decarburization in an on-line dynamic model. He stated that it is disadvantageous to have a high fraction of liquid slag during the decarburization. In the present study an attempt was made to show how the physical aspects of the slag can affect the decarburization.

A computer model previously developed [2] and later augmented with chemical reactions [3] has now been used to investigate the influence of slag on the decarburization. In the present study, an industrial AOD converter has been modeled. More specifically, the first stage of injection has been simulated for different amounts of top slag and slag separation of solid chromium oxide to the liquid slag. This investigation focused on the effect of top slag amount on the refining of carbon in the converter. Mainly, the pressure effect of the shear amount of top slag was investigated. Furthermore, a study was made on how the separation of solid chromium oxide to the liquid slag emulsified in the steel bath affects the chromium losses. The emulsified chromium oxide was considered inert for further reactions. Overall, this study represents a novel approach to obtain further information on the AOD process.

2. Numerical Model

The computational domain together with the gas hold-up and the main flow can be seen in Figure 1. The tuyeres are located at the bottom-left part of the converter.

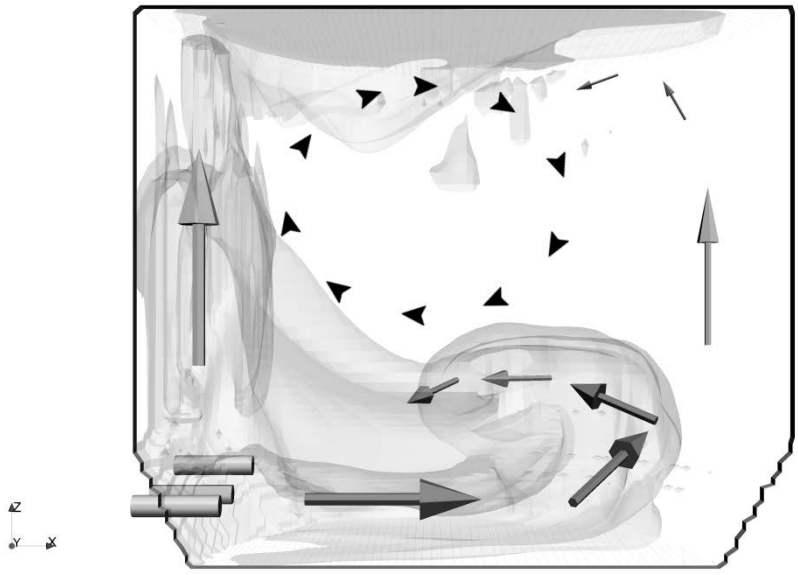

Figure 1. Shows domain shape together with main flow and gas fraction.

2.1 Transport Equations

The flow field was obtained from a previous work by solving the equations in the three-dimensional three-phase fluid flow model of gas injection in the AOD converter [2]. In addition, the following transport equation is used for transport of any species, ϕ_i^k of phase, *i*:

$$\frac{d\left(\alpha_i \rho_i \phi_i^k\right)}{dt} + \boldsymbol{\nabla} \cdot \left(\alpha_i \rho_i \boldsymbol{v}_i \phi_i^k\right) = \boldsymbol{\nabla} \cdot \left(\alpha_i \rho_i \left(D_0^k + \frac{\mu_t}{\rho_i \mathrm{Sc}_t}\right) \boldsymbol{\nabla} \phi_i^k\right) \quad (1)$$

where α_i is the phase volume fraction, ρ_i is the phase density, t is the time, $\boldsymbol{v}_i$ is the phase velocity vector, D_0^k is the diffusion coefficient for specie k, μ_t is the turbulent dynamic viscosity and Sc_t is the turbulent Schmidt number (here assumed =1).

2.2 Properties

The liquid phase consists of both steel and liquid slag. The steel and slag temperature is assumed to follow the linear relation:

$$T = \mathrm{t} \cdot 0.4709 + 1831.7\ [K] \qquad (2)$$

where *t* is the simulated time in seconds. The linear relation is obtained by a regression of data from the TimeAOD2 model [4]. The latter takes temperature into consideration, including heat from reactions as well as cooling effects of gas and slag. During the calculations, density and viscosity of gas, steel and slag are functions of temperature. For further details it is referred to Tilliander et al [2].

The metallostatic pressure in a cell is calculated considering the amount of gas that is located above it, using a mean density value. The top slag inflicts an additional force on the steel bath that will increase the metallostatic pressure of the overall bath. Further terms are added to account for bubble-drag, bubble-swarm drag and for the cavity just outside the tuyeres [2].

2.3 Thermodynamics

Thermodynamic calculations are done using the Thermo-Calc [5] software version S. Moreover, the databases *TCMSI1*[6] and *SSUB4* [7] are used for liquid together with slag and gas, respectively. Thermo-Calc is a general software package for multi-component equilibrium calculations, using minimization of the Gibbs free energy for equilibrium computations. It allows for flexible setting of conditions for the equilibrium state. Thus, it is suitable for the presented process simulations.
A combined equilibrium between formation of chromium oxide and carbon monoxide can be written as:

$$Cr_2O_3(s) + 3\underline{C} = 3CO(g) + 2\underline{Cr} \qquad (3)$$

Firstly, the enthalpy content is calculated for each compound separately. Secondly, the heat content is summed up and set as an input argument for the total equilibrium calculation. Finally, the new compositions and amounts of the compounds are obtained.

The thermodynamic system used in this investigation consists of the elements *Fe*, *Cr*, *Ni*, *C* and *O*. The system is divided into gas, liquid as well as the possible oxides of all the elements *FeO*, Fe_2O_3, Fe_3O_4, Cr_2O_3 and *NiO*. Conditions for pressure, temperature, composition fractions and phase masses are taken as input from the unsteady CFD solution. For the

gas, the species are transported in order to keep track of the oxygen in all the phases. More specifically, the gas species transported are O_2, CO and CO_2.

2.4 Coupling

The interface between Thermo-Calc and PHOENICS is a FORTRAN application programming interface known as TQ [5]. This is an interface within the Thermo-Calc software package that can implement functions in the native language of Thermo-Calc. This enables a reasonably quick handling of functions for the thermodynamic calculations.

The CFD model computes the convection and diffusion of reaction products and elements. Thereafter, thermodynamic calculations are made in each horizontal grid-plane cell-wise, if the conditions are met. Reactions take place if the gas volume is between 20-99.5% in a calculation cell. Equilibriums are calculated at the beginning of each time step and when the gas composition has changed by 5 wt-% units or more. The reaction products and elements are then updated for another convection and diffusion transport in the CFD model.

2.5 Formulation, boundary conditions and method of solution

In the declaration of the model the following statements are made:

a) The computational grid is Cartesian in a cuboid domain with the dimensions $3 \times 1.7 \times 2.37$ m divided into $78 \times 44 \times 56$ volume elements.
b) A symmetry condition exists along the center plane of the converter at Y=0 for the XZ-plane domain limit.
c) The free surface is flat. In addition, the gas bubbles are allowed to leave the domain through the surface.
d) A standard logarithmic log-law is used for the walls and bottom of the converter, with the roughness 0.0025 m.
e) At inflow boundaries the gas flow rates are constant at 20 m^3/min (STP) for each of the three inlets.
f) The discretization scheme used is Elliptic-Staggered. The differencing scheme used is hybrid.
g) A converged flow field was obtained earlier [2]. Using this flow field scalar transport was used to transport the thermodynamic quantities and the flow field itself remained constant.
h) The model considers the three phase system steel, liquid slag and gas.
i) Thermodynamic equilibrium is assumed to be reached in every cell for every time step.
j) Only the initial injection stage is considered where the injected gas is assumed to be 100% O_2.
k) The steel temperature is assumed to increase linearly according to a regression of TimeAOD2 data [4].
l) The injected gas adopts the steel temperature momentarily.
m) Computation starts at the beginning of decarburization and is terminated when the steel temperature reach 2000 K.
n) No cooling scrap is considered.
o) The reactions taking place include the following elements: *Fe*, *Cr*, *Ni*, *C* and *O*.

The calculations were performed using the commercial software PHOENICS [8]. The solution was made in a transient mode using 3 200 number of 0.125 seconds time-steps. A typical calculation took about 72 hours on a standard pc, core i7 at 3.0 GHz.

3. Results

3.1 Top slag

The carbon concentration, shown in Figure 2, shows a clear vertical translation starting at the 1 minute mark. The effect of top slag amount does not seem to have a great effect on the decarburization, although a clear tendency can be seen that an increased amount of top slag decreases the decarburization rate. A difference of about 30s can be seen between large and small amounts of top slag.

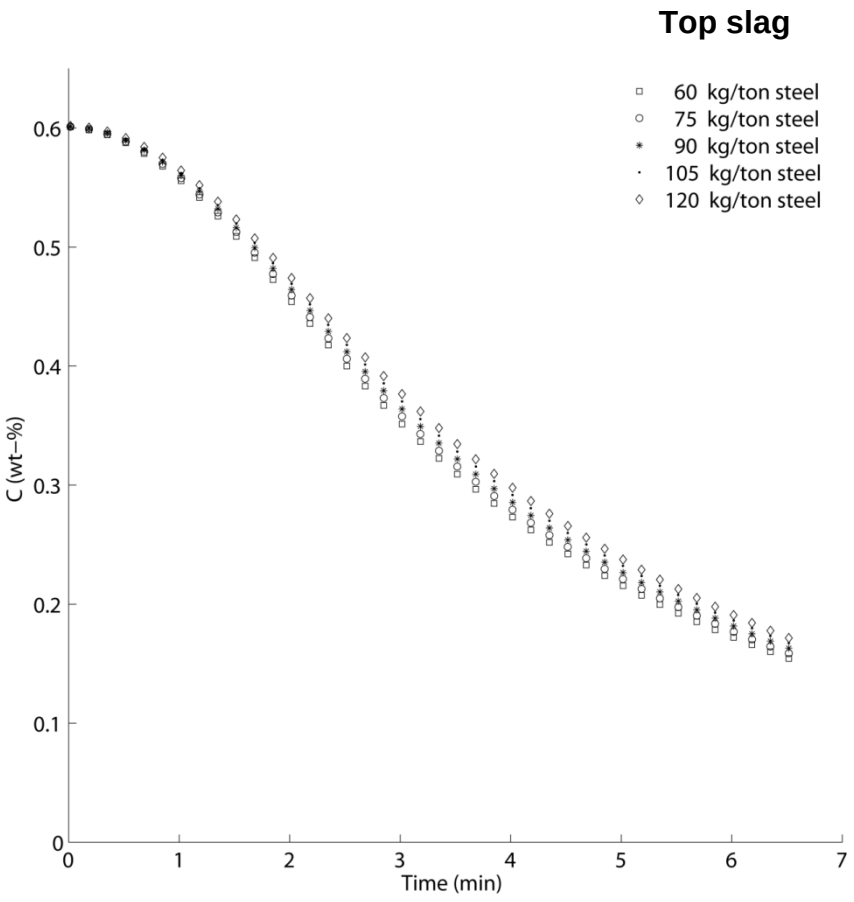

Figure 2. A graph of carbon concentration over time, for different amounts of top slag.

The carbon removal efficiency (CRE) can be seen in Figure 3 for different amounts of top slags. Here it can be seen that with a large amount of top slag the CRE maxima is decreased by 10% units compared to a case with a low amount of top slag. Also, towards the end of the first injection step it is indicated that the CRE is higher for a case with a large amount of top slag and lower for a case with a small amount of top slag.

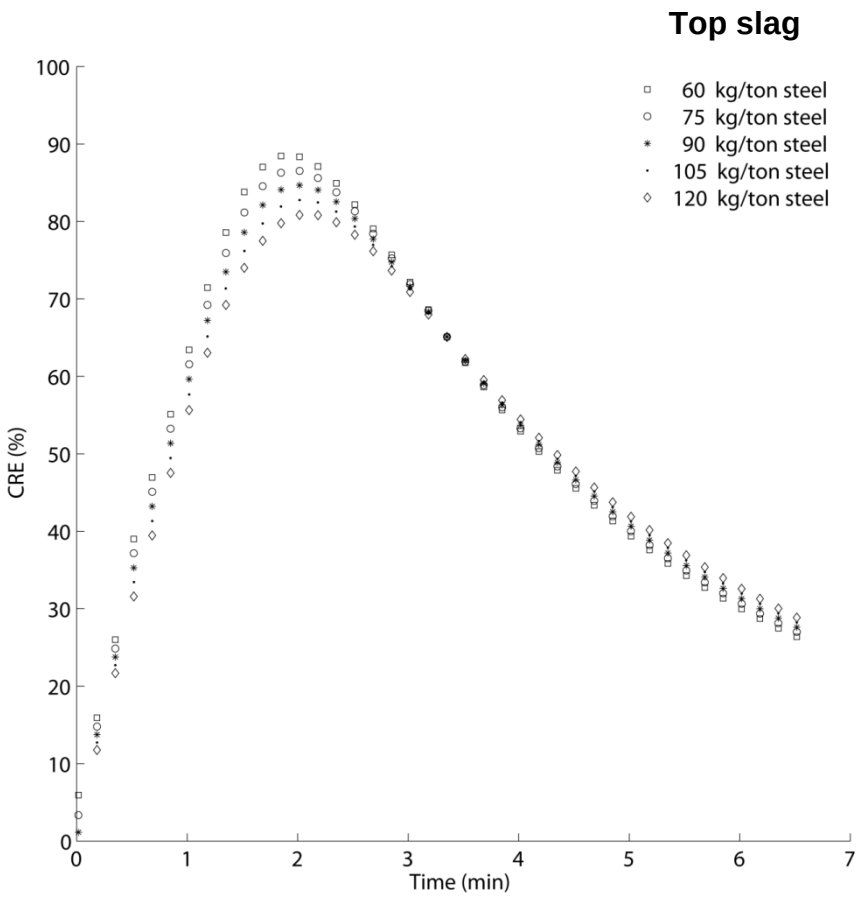

Figure 3. A graph of carbon removal efficiency over time, for different amounts of top slag.

Figure 4, shows the dissolved oxygen concentration. The concentration of dissolved oxygen is predicted to increase from around 130 ppm to 470 ppm during the process. However, the dissolved oxygen does not seem to be affected by the amount of top slag.

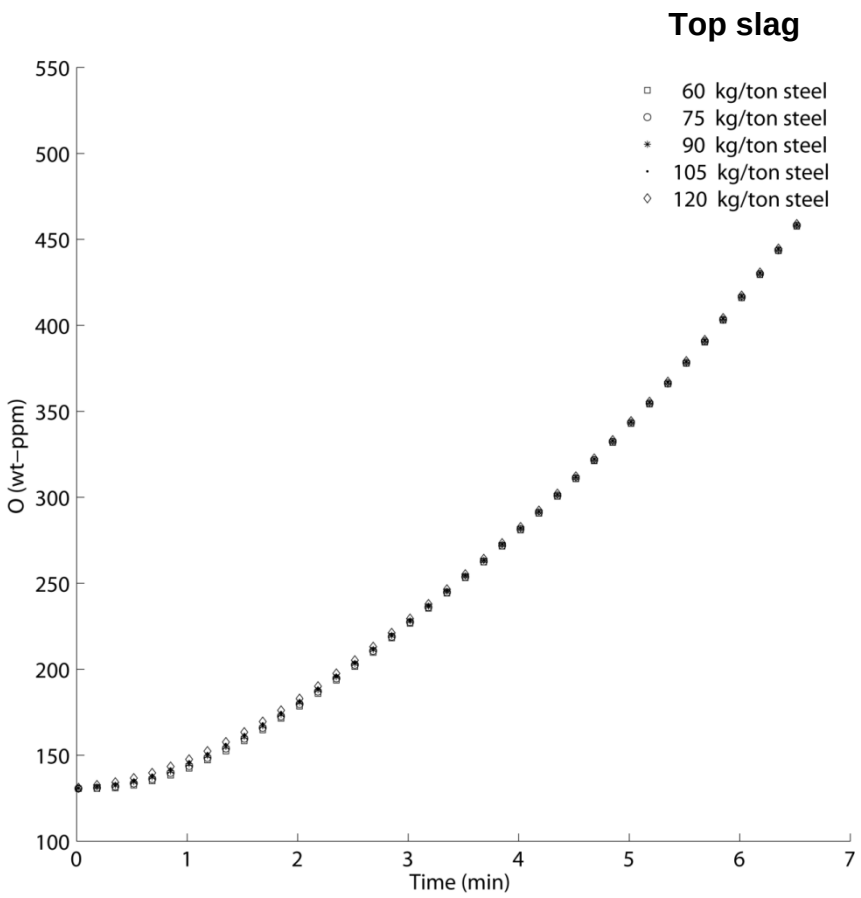

Figure 4. A graph of dissolved oxygen concentration over time, for different amounts of top slag.

3.2 Slag separation

Figure 5, shows the carbon concentration for different ratios of slag separation. The differences between the curves are most prominent in the middle part of the curve where the decarburization is largest. However, at around 4 minutes the curves seem to converge towards the same concentration.

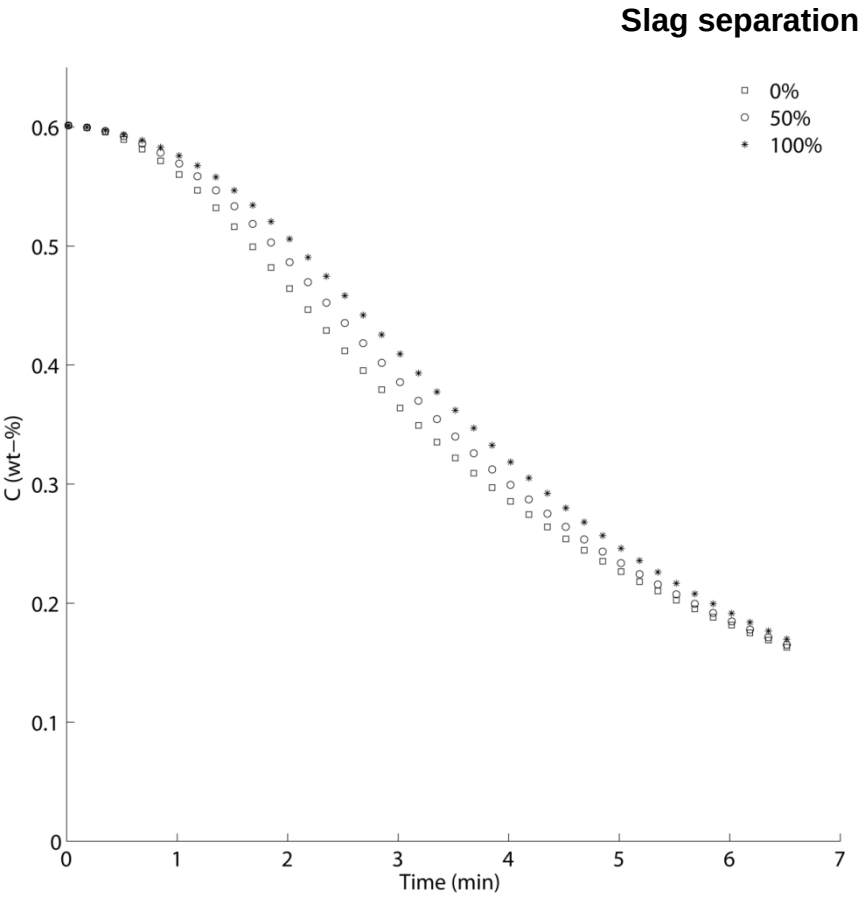

Figure 5. A graph of carbon concentration over time, for different ratios of slag separation.

The CRE can be seen in Figure 6. The initial increase of the CRE value is lower for higher degrees of slag separation. Furthermore, with higher slag separation ratios the CRE maximum is pushed towards longer times. The maximum for a 0% slag separation is around 2 min, while a 50% slag separation is roughly 2.5 min and 100 % slag separation is around 3 min. The descending from the maximum is fastest for the 0% slag separation, while slowest decrease for the 100% slag separation.

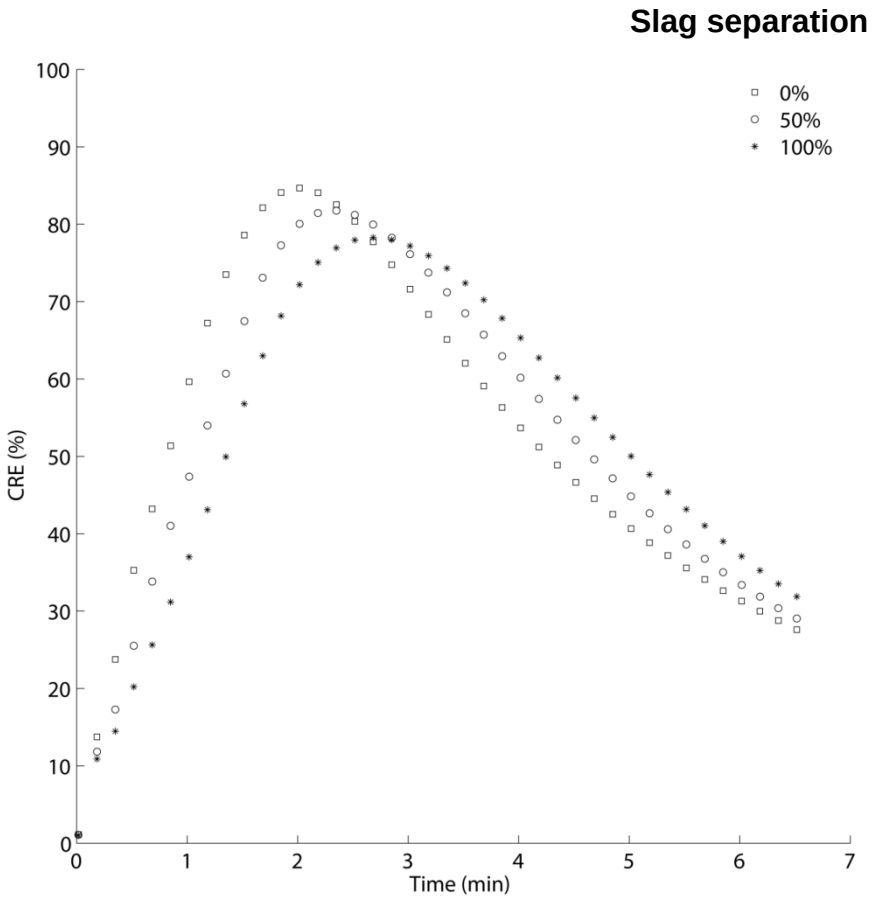

Figure 6. A graph of carbon removal efficiency over time, for different ratios of slag separation.

The dissolved oxygen concentration is shown in Figure 7. It is indicated that for a period from about 1 min to 5 min, for which the increase of dissolved oxygen is different. With more slag separation there is a predicted trend that the dissolution of oxygen is lower than for no slag separation. The largest difference of about 25 ppm occurs around 3 min.

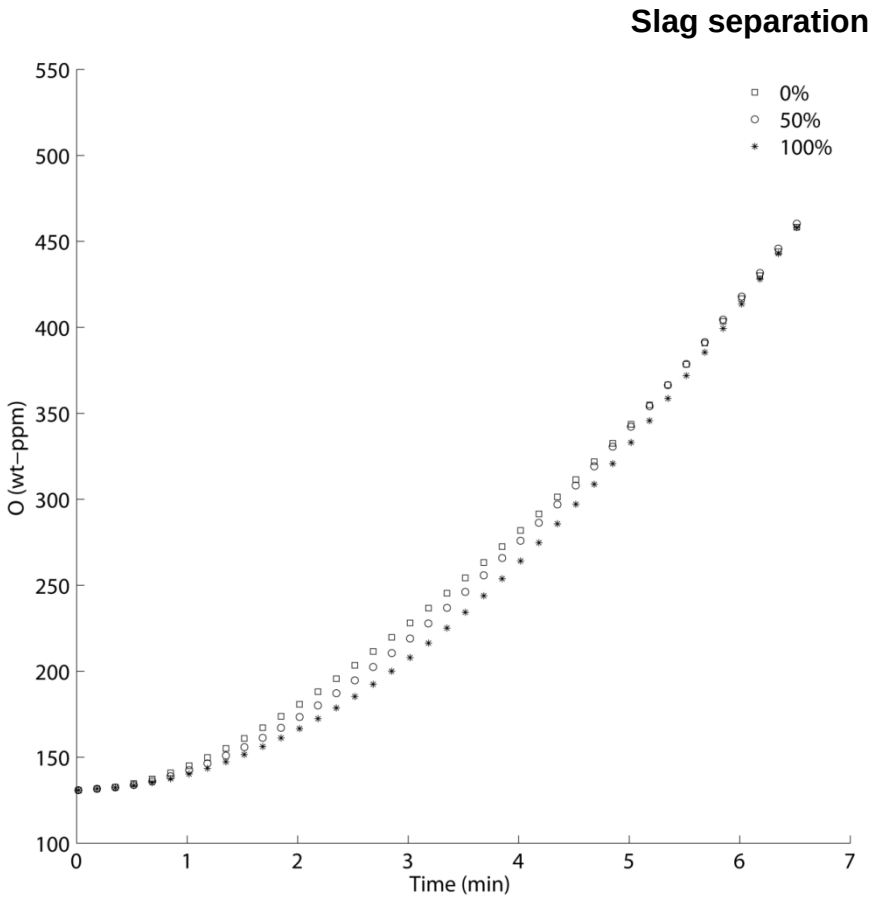

Figure 7. A graph of dissolved oxygen concentration over time, for different ratios of slag separation.

4. Discussion

Figure 3, suggested that the CRE tendency at the maxima fortified carbon removal for low amounts of top slag. However, at the end the CRE tendencies were reversed. The trend for the maxima can be seen as utilization of depth of the converter. With a large amount of top slag the critical pressure for reaction (3) equals a depth that is less than for small amounts of top slag. Thus, a greater part of the converter is used for decarburization for smaller amounts of top slag. For the case with large amount of top slag the carbon is higher towards the end. This is a consequence due to the reduced decarburization earlier. A higher carbon concentration (Figure 2) is obtained at longer process times and is more inclined to react at the increased temperature. Therefore, the CRE is slightly higher than for the case with a low amount of top slag.

The carbon concentration (Figure 5) for the slag separation investigation separate at an early stage and join together at 6.5 min. This can be seen in the corresponding CRE data (Figure 6), where the areas under the curves are about the same. Thus, it is logical that the carbon concentrations converge at the end.

The effect of the top slag on decarburization increases with time, while the effect of slag separation first reaches a maximum effect and thereafter decreases. However, if one examine the magnitudes it is dubious if any of these phenomena have significant effect on decarburization in the process. Though, minimizing the amount of liquid slag would indeed decrease the slag separation phenomena. However, if the ratio of slag separation can be verified, this may give information for a suitable time to change the injection step, so it happens at an optimal time with respect to the decarburization reaction (3).

5. Conclusions

A study of the effect of the slag on decarburization in an industrial AOD converter with six tuyeres has been carried out using mathematical modeling. Initially, the flow field was obtained from an existing mathematical model which solves the transport equations in three dimensions as well as for three phases. The top slag was considered due to its overall increase of the metallostatic pressure in the melt. Furthermore, the influence of the slag separation on the decarburization was studied. Overall, the results show some trends how the slag affects the decarburization in a non-chemical way. The main findings can be summarized as follows:

- A higher CRE value is achievable if the amount of top slag can be reduced.
- The CRE maximum is delayed by the degree of slag separation.
- It is dubious in this study if the amount of top slag has a significant effect on the final carbon concentration after the final injection step.

Acknowledgements

In addition, the authors would like to thank Mr. Gunnar Lindstrand of Outokumpu Stainless as well as Mr. Patrik Ternstedt of Kobolde for helpful discussions.

References

[1] P. Ternstedt, R. Gyllenram, J. Bengtsson, P. G. Jönsson. Using an AOD simulator workbench to support process control development. METEC INSTEELCON PROC., 27 June – 1 July, 2011 (Düsseldorf).

[2] A. Tilliander, T. L. I. Jonsson, P. G. Jönsson: KTH-ISBN 978-91-7501-266-7.

[3] N. Andersson, A. Tilliander, T. L. I. Jonsson, P. G. Jönsson: KTH-ISBN 978-91-7501-267-4.

[4] TimeAOD2 process control model, created by Pontus Sjöberg, further enhanced and developed by Patrik Ternstedt at Kobolde & Partners AB.

[5] J.-O. Andersson, T. Helander, L. Höglund, P. Shi, B. Sundman: Calphad, **26**(2002), 273.
[6] TCMSI1: TCS Metal Slag Interaction Database, Version 3.0, May 2009, Thermo-Calc Software AB.
[7] SSUB4 - SGTE Substances Database, Version 4.1, Aug. 2008, Scientific Group Thermodata Europe.
[8] PHOENICS 2008, “The PHOENICS-VR reference guide”, CHAM TR 326.